Structure, Vol. 12, 417–428, March, 2004, ©2004 Elsevier Science Ltd. All rights reserved. DOI 10.1016/j.str.2004.02.008

Cofactor-Induced Conformational Rearrangements Establish a Catalytically Competent Active Site and a Proton Relay Conduit in FabG

Allen C. Price,[1] Yong-Mei Zhang,[2] Charles O. Rock,[2,3] and Stephen W. White[1,3,*]

[1]Department of Structural Biology
[2]Department of Infectious Diseases
St Jude Children's Research Hospital
Memphis, Tennessee 38105
[3]Department of Molecular Sciences
University of Tennessee Health Science Center
Memphis, Tennessee 38163

Summary

β-Ketoacyl-acyl carrier protein reductase (FabG) is a key component in the type II fatty acid synthase system. The structures of *Escherichia coli* FabG and the FabG[Y151F] mutant in binary complexes with NADP(H) reveal that mechanistically important conformational changes accompany cofactor binding. The active site Ser-Tyr-Lys triad is repositioned into a catalytically competent constellation, and a hydrogen bonded network consisting of ribose hydroxyls, the Ser-Tyr-Lys triad, and four water molecules creates a proton wire to replenish the tyrosine proton donated during catalysis. Also, a disordered loop in FabG forms a substructure in the complex that shapes the entrance to the active site. A key observation is that the nicotinamide portion of the cofactor is disordered in the FabG [Y151F]·NADP(H) complex, and Tyr151 appears to be necessary for high-affinity cofactor binding. Biochemical data confirm that FabG[Y151F] is defective in NADPH binding. Finally, structural changes consistent with the observed negative cooperativity of FabG are described.

Introduction

The de novo synthesis of fatty acids occurs by a series of universal biochemical transformations that are critical to almost all cells. There are two distinct architectures for the fatty acid synthase system. The type I system is found in metazoans and consists of a multifunctional complex in which all the catalytic activities are fused into a single large polypeptide chain (Smith et al., 2003). In contrast, bacteria and plants contain the type II (FAS II) system in which the catalytic activities reside on individual protein molecules encoded by separate genes (Cronan and Rock, 1996; Jackowski and Rock, 2002). Although all of the chemical reactions are the same and most of the active site sequences in FAS I and II are related, important differences between the systems have been exploited in the development of FAS II as a target for drug discovery (Campbell and Cronan, 2001; Heath et al., 2001). Potent antibacterials that act by inhibiting FAS II include isoniazid, triclosan, cerulenin, and thiolactomycin.

*Correspondence: stephen.white@stjude.org

The core reactions of FAS II occur in the elongation cycle that repeatedly extends the acyl chain by two-carbon units (Cronan and Rock, 1996; Jackowski and Rock, 2002). The elongating substrate is attached as a thioester to the terminal sulfhydryl of the 4′-phosphopantetheine moiety of acyl carrier protein (ACP), and the growing acyl chain is carried by ACP to a series of four enzymes. First, a β-ketoacyl-ACP synthase (FabB or FabF) elongates the acyl-ACP C_n acyl chain to a C_{n+2} β-ketoacyl form. Next, the β-keto group is reduced by the NADPH-dependent β-ketoacyl-ACP reductase (FabG, the subject of this study), and the resulting β-hydroxy intermediate is then dehydrated by the β-hydroxy acyl-ACP dehydratase (FabA or FabZ) to an enoyl-ACP. Finally, the reduction of the enoyl chain by a nucleotide cofactor-dependent enoyl-ACP reductase (FabI, FabK, or FabL) produces an acyl-ACP with an elongated C_{n+2} acyl chain, which is ready to reenter the cycle. FabG requires NADPH for its activity (Alberts et al., 1964; Toomey and Wakil, 1966), has a monomeric molecular weight of 25.5 kDa, and exists as a tetramer in solution (Sheldon et al., 1992). FabG operates by a sequential, ordered kinetic mechanism in which the reduced cofactor is the first substrate to bind to the enzyme and the oxidized cofactor is the last to leave (Fawcett et al., 2000; Price et al., 2001). The primary sequence of FabG reveals that the protein belongs to the short-chain dehydrogenase/reductase (SDR) family of enzymes, whose members catalyze a broad range of reduction and dehydrogenase reactions using a nucleotide cofactor (Jörnvall et al., 1995; Oppermann et al., 2003). FabG is ubiquitously expressed in bacteria (Zhang and Cronan, 1998), is highly conserved across species, and is the only known protein isoform that functions as a keto reductase in the FAS II system. Therefore, it is somewhat surprising that FabG has not been developed as a target for new drug discovery, although the enzyme appears to represent an ideal target for the development of new antibiotics (Campbell and Cronan, 2001; Heath et al., 2001).

We recently determined the crystal structure of FabG from *E. coli* and found that the side chains of the active site residues (Ser138, Tyr151, and Lys155) were in a nonproductive conformation (Price et al., 2001), leading to the prediction that FabG undergoes significant conformational changes prior to catalysis. During the catalytic reaction, the β-keto group is reduced to a β-hydroxy group by a hydride ion from the nicotinamide cofactor and a proton most likely donated by the hydroxyl of Tyr151, based on the similarity of FabG to other SDR family members (Oppermann et al., 2003). Most of these SDR family members whose structures are known do not undergo a rearrangement of the active site residues upon cofactor binding. Furthermore, FabG also exhibits negative cooperativity (Price et al., 2001). The binding of NADPH to one site increases the affinity at that site for ACP and simultaneously decreases the affinity for the cofactor at other sites. In this study, we report the structures of FabG and the FabG[Y151F] mutant in com-

Table 1. Data Collection Statistics

Protein	FabG·NADP$^+$	FabG[Y151F]·NADP(H)
Space group	$P2_1$	$C222_1$
Unit cell dimensions (Å) (a, b, c)	72.7, 76.2, 99.7	75.9, 95.9, 131.6
Unit cell angles (°) (α, β, γ)	90, 109.5, 90	90, 90, 90
Resolution range (Å)	20.0–2.05 (2.09–2.05)[a]	65.8–2.50 (2.61–2.50)
Multiplicity	2.8 (2.5)	10.1 (7.9)
R_{sym}[b]	0.044 (0.356)	0.057 (0.174)
I/σ	24.3 (2.26)	9.41 (3.40)
Completeness (%)	95.3 (90.9)	99.95 (100.0)
Reflections	306191	172466
Unique reflections	64081 (2888)	17095 (2163)

[a] Values in parentheses refer to the highest resolution shell.
[b] $R_{sym} = \Sigma\Sigma|I_i - I_m|/\Sigma\Sigma I_i$, where I_i is the intensity of the measured reflection, and I_m is the mean intensity of all symmetry related reflections.

plex with NADP(H). These new structures, along with the FabG structure reported previously, allow us to define structural mechanisms that mediate the allosteric behavior of FabG. Key differences in the conformation of the cofactor observed in the structures of the wild-type and mutant binary complexes reveal a two-step binding mechanism for the cofactor. This binding leads to the reorganization of the active site residues into a catalytic-competent conformation and to the establishment of a proton relay conduit to replenish the Tyr151 proton donated to the substrate during catalysis.

Results

Quality of the Structures

Analyses of the final structures, performed using PROCHECK (Laskowski et al., 1993) and CNS v1.1 (Brünger et al., 1998), show the overall stereochemical statistics to be very good for both structures (Tables 1 and 2). The final R factors for FabG·NADP$^+$ ($R_{test} = 0.221$, $R_{work} = 0.200$) and for FabG[Y151F]·NADP(H) ($R_{test} = 0.252$, $R_{work} = 0.215$) are excellent values for structures at 2.1 Å and 2.5 Å resolution, respectively. In the FabG·NADP$^+$ structure, only the N-terminal methionines in monomers A, B, and D were not visible in the final electron density. In FabG[Y151F]·NADP(H), the only residues not visible in the electron density were the N-terminal methionines of monomers A and B. The quality and extent of the cofactor electron density was different in the wild-type and mutant structures. In the wild-type structure, the density for the entire cofactor was clearly defined, but the density defining the adenine and adenine ribose was significantly stronger than that of the nicotinamide and its associated ribose. In the FabG[Y151F]·NADP(H) structure, the adenine and adenine ribose moieties were well defined, but the complete absence of density for the nicotinamide and the nicotinamide ribose showed that this part of the cofactor is disordered in the mutant complex.

Description of the Crystal Forms

Although the crystal forms are different, the structures of the FabG·NADP$^+$ and FabG[Y151F]·NADP(H) complexes are virtually identical. Only localized differences in the binding of the cofactor were noted. Therefore, the figures and discussion that follow refer to the higher resolution FabG·NADP$^+$ structure. The overall fold adopted by the binary complex is shown in Figure 1A and is essentially the same as the *E. coli* FabG structure we reported and discussed previously (Price et al., 2001). Briefly, the protein adopts a Rossmann fold. The core is composed of a twisted, parallel β sheet of seven β

Table 2. Statistics of Refinement

Protein	FabG·NADP$^+$	FabG[Y151F]·NADP(H)
Resolution range included	20.0–2.05	65.8–2.50
Number of reflections in working set	57920	14740
Number of reflections in test set	3083	1641
Number of protein atoms in ASU[a]	7809	3558
Number of cofactor atoms in ASU	192	62
Number of water molecules in ASU	502	92
R_{work}	0.200	0.215
R_{test}	0.221	0.252
Rmsd from ideal stereochemistry		
Bond lengths (Å)	0.007	0.007
Bond angles (°)	1.18	1.17
Mean B (main chain) (Å^2)	31.2	24.0
Mean B (side chains, waters) (Å^2)	34.9	28.5
Mean B (cofactor) (Å^2)	39.6	75.8
Ramachandran plot		
Most favored region (%)	91.8	92.6
Additionally allowed region (%)	8.2	7.4

[a] ASU means asymmetric unit.

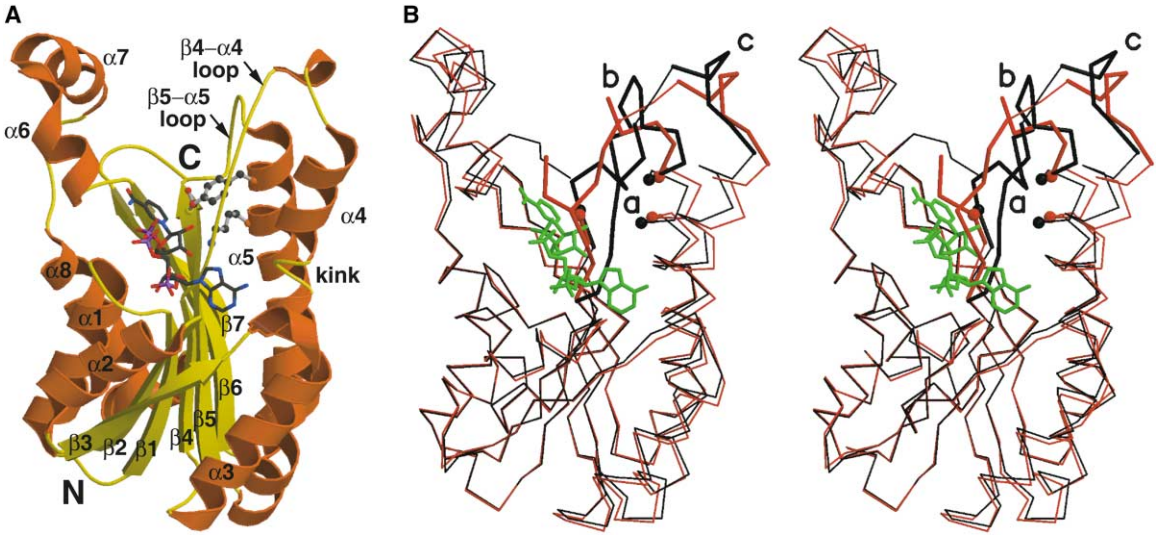

Figure 1. The FabG·NADP$^+$ Binary Complex

(A) Overview of the complex. α helices are orange, and β strands and coil regions are yellow. The three active site residues, Ser138, Tyr151, and Lys155, are shown as ball-and-stick figures. The NADP$^+$ cofactor is shown as a stick figure with carbons colored gray, nitrogens blue, oxygens red, and phosphorous purple. The secondary structure elements, and selected loop regions that are discussed in the paper, are labeled.

(B) A stereo view overlay of the FabG·NADP$^+$ binary complex (black) and the FabG structure (red) in the same orientation as (A). The structures are shown as α-carbon traces, and NADP$^+$ is illustrated as a green stick figure. The regions of major conformational change are emphasized with bold. The locations of the active site residues are shown as black spheres. Region "a" is the strand which overlaps the Tyr151 side chain in the FabG structure. Region "b" is disordered in the FabG structure, but forms a short α helix in the binary complex. Region "c" is involved in intermolecular contacts at the monomer-monomer interface. Both figures were produced using MOLSCRIPT (Kraulis, 1991) and rendered with RASTER3D (Merritt and Murphy, 1994).

strands covered on both sides by a total of eight α helices. Two right-handed βαβαβ motifs make up the center of the structure, and helix α3 connects these two motifs. The first motif is composed of strands, β1, β2, and β3 and helices α1 and α2, and the second is made up of strands β4, β5, and β6 and helices α4 and α5. Helices α6 and α7 form a small helix-turn-helix subdomain distinct from the body of the protein, and the final two secondary structure elements, α8 and β7, rejoin the body of the protein at the edge of the β sheet adjacent to strand β6.

The crystal form of the FabG·NADP$^+$ complex contains one tetramer in the asymmetric unit. Each of the four monomers in the asymmetric unit adopts the same fold with minor differences due to crystal contacts. The largest such differences are on the order of 1 Å in the α6/α7 subdomain. The α6/α7 subdomain (residues 185–200) has significantly higher B factors than the rest of the protein, indicating that it is a flexible region of the molecule. Each monomer in the complex binds to one NADP$^+$ molecule in an identical manner. In addition to the four NADP$^+$ molecules, the asymmetric unit also contains eight Ca^{2+} ions. The crystal form of the FabG[Y151F]·NADP(H) complex contains two monomers in the asymmetric unit. Each monomer is identical apart from minor differences involving crystal contacts. The biologically relevant tetramer is formed by a crystallographic 2-fold axis parallel to the crystallographic *b*-axis. Each monomer contains a single NADP(H) molecule bound in an identical manner. As noted earlier, the nicotinamide and associated ribose of each NADP(H) molecule are disordered and not visible in the electron density.

FabG-Cofactor Interactions in the FabG·NADP$^+$ Complex

The detailed interactions between FabG and the cofactor in the FabG·NADP$^+$ complex are shown in Figure 2. The cofactor is in the *syn* conformation, and it straddles the β sheet topological switch point at the divergence of the two β strands, β1 and β4 (Figure 1A). The adenine moiety and its associated ribose are situated in a cleft some distance from the active site bounded by four loop regions, β1-α1, β2-α2, β3-α3, and β4-α4, and helix α4. The adenine ring is secured by two direct hydrogen bonds, from the extracyclic amino nitrogen at the C6 position to the OD1 atom of Asn59 and from the ring N1 nitrogen to the amide nitrogen of Val60. Also, there are indirect hydrogen bonding interactions via water molecules from the amino nitrogen to the OG1 atom of Thr109, and from the N3 nitrogen to the OG1 atom of Thr35 and to the main chain carbonyl oxygen of Leu58. The adenine ribose phosphate group is held in place by hydrogen bonding interactions with the OG and OG1 atoms of Ser14 and Thr37, respectively, as well as a salt bridge interaction with Arg15. The pyrophosphate is secured by a salt bridge with Arg15 and by a hydrogen bond with the amide nitrogen of the nicotinamide group. There are two bridging water molecules that form hydrogen bonds with two pyrophosphate oxygens on one side and with the protein backbone on the other (not shown in Figure 2 for clarity). The nicotinamide and its

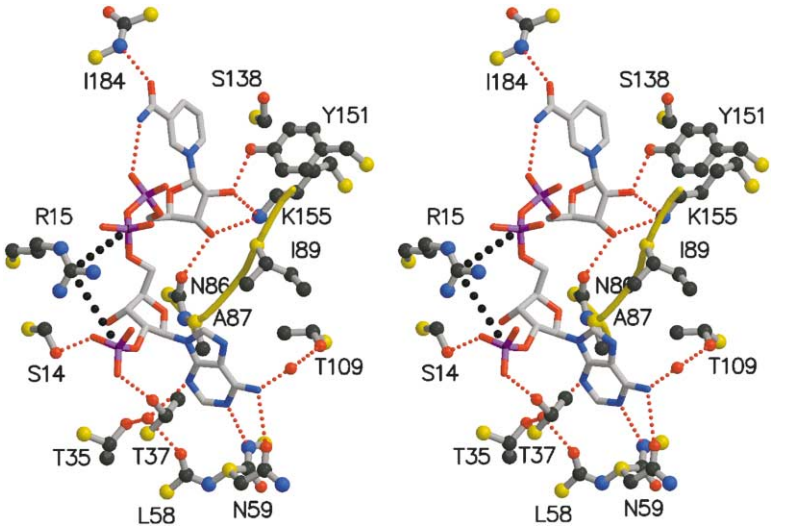

Figure 2. Ligand-Protein Interactions in the FabG·NADP$^+$ Complex

In this stereo view, only individual residues and waters that make specific contacts with the NADP$^+$ are shown. For clarity, only backbone atoms are shown where necessary, and the α-carbons are colored yellow. The adenine is bound by interactions with two waters and by direct hydrogen bonds to Asn59 and to a backbone nitrogen. The "back" of the adenine pocket is created by the N-terminal region of the β4-α4 loop (shown as a yellow coil) and the side chains of the component residues, Ala87 and Ile89. The adenine ribose phosphate is stabilized by ionic interaction with Arg15 and hydrogen bonds to Ser14 and Thr37. The pyrophosphate forms an ionic interaction with Arg15 and an intramolecular hydrogen bond to the amide nitrogen of NADP$^+$. The nicotinamide ribose is bound by hydrogen bonds to two active site residues, Tyr151 and Lys155. The nicotinamide is held by two hydrogen bonds, the intramolecular bond to the pyrophosphate, and the hydrogen bond to the backbone amide nitrogen of I1e84. Hydrogen bonds are shown as dotted red lines, and ionic interactions are shown by large black dotted lines. The figure was produced using MOLSCRIPT (Kraulis, 1991) and rendered with RASTER3D (Merritt and Murphy, 1994).

associated ribose are located near the active site at the base of a hydrophobic cleft, and the two ribose hydroxyl groups are involved in four hydrogen bonding interactions. The 2′-hydroxyl bonds to the hydroxyl of Tyr151 and to the NZ atom of Lys155, and the 3′-hydroxyl bonds to the main chain carbonyl oxygen of Asn86 and to the NZ atom of Lys155. Note that the nicotinamide ribose interacts directly with two active site residues, Tyr151 and Lys155. There is also a hydrogen bond between the nicotinamide amide oxygen and the main chain amide nitrogen of Ile184.

FabG-Cofactor Interactions in the FabG[Y151F]·NADP(H) Complex

Compared to the wild-type complex, the cofactor is bound differently to the FabG[Y151F] point mutant, and this is shown in Figure 3A, where the two conformations are superimposed. Although the adenine, adenine ribose, and adenine ribose phosphate groups all form the same interactions, the pyrophosphate is bound in a different position, and the nicotinamide and nicotinamide ribose are disordered and not visible in the FabG[Y151F]·NADP(H) electron density. This important difference was verified by calculating simulated annealing omit maps in which the cofactors were removed from the two structures. The different binding modes of the pyrophosphate conserve one salt bridge interaction between the phosphate closest to the adenine ribose and Arg15, but the second phosphate group is removed from its location near the active site and interacts with Arg91, which lies outside the cofactor binding cleft. This binding mode in FabG[Y151F]·NADP(H) results in the NADP(H) adopting a catalytically nonproductive conformation in which the nicotinamide group is not bound in the active site.

These structural differences between the two complexes suggest that the two active site residues Tyr151 and Lys155 play key roles in promoting the binding of the nicotinamide "half" of the cofactor by providing hydrogen bonding interactions with the ribose moiety. This was directly tested by measuring the binding of NADPH to the wild-type and mutant proteins. The results are shown in Figure 3B and are completely consistent with this scenario. Whereas FabG bound NADPH with a Kd of 3.5 μM calculated from the binding curve, neither the FabG[Y151F] or FabG[K155A] mutant proteins bound a significant amount of NADPH at the concentrations tested. Thus, the mutant proteins have a defect in the affinity for NADPH. Mutations of the lysine component of the catalytic triad lead to reduced cofactor affinity (Tanabe et al., 1998), and the model for cofactor binding in SDR proteins always defines a role for the lysine in high-affinity interactions with the ribose hydroxyls of the cofactor (Jörnvall et al., 1995; Oppermann et al., 2003). Although mutation of the active site tyrosine uniformly inactivates SDR family proteins (Oppermann et al., 2003), where binding was examined, tyrosine to phenylalanine mutations did not affect NADPH affinity (Filling et al., 2002; Tanabe et al., 1998). However, many of these SDR family members do not undergo a conformational change in active site geometry upon cofactor binding (Ghosh et al., 1995; Grimm et al., 2000; Somoza et al., 2000), which suggests that the tyrosine interaction with the cofactor is a more important contributor to stabilizing the FabG·NADPH binary complex than in the formation of the same binary complex in other SDR family members.

Cofactor-Induced Conformational Changes

A comparison of the FabG·NADP$^+$ structure to the FabG structure (Price et al., 2001) reveals that significant conformational changes occur upon cofactor binding (Figure 1B). The conformational differences are restricted to four distinct regions, the active site, the β4-α4 loop between residues 87 and 91 (labeled "a" in Figure 1B), the β5-α5 loop between residues 141 and 146 (labeled "b" in Figure 1B), and at a specific location on the dimer interface (labeled "c"). These changes are functionally

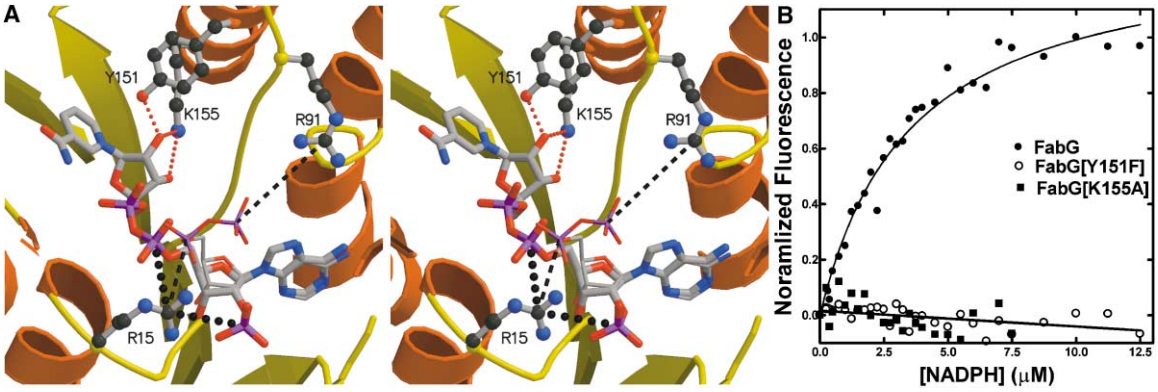

Figure 3. Cofactor Binding to FabG and to FabG[Y151F]

(A) A stereo view showing an overlay of the modes of binding of the $NADP^+$ molecule to FabG and to FabG[Y151F]. In both cases, $NADP^+$ carbons are colored gray, nitrogens blue, oxygens red, and phosphorous purple. The $NADP^+$ is drawn with thicker bonds in the wild-type complex. The secondary structural elements of the protein are colored as in Figure 1A. The protein side chains in the two complexes are in identical conformations. The adenine and adenine ribose moieties bind in the same manner in the wild-type and mutant proteins, while the pyrophosphate groups diverge. The catalytically nonproductive conformation observed in the FabG[Y151F]·$NADP^+$ structure is stabilized by a salt bridge interaction with Arg91 that is not present in the wild-type complex. The nicotinamide moiety of the cofactor is completely disordered in the FabG[Y151F]·$NADP^+$ complex. Hydrogen bonds are shown as dotted red lines, and salt bridge interactions are shown as dashed black lines. The latter are thicker in the wild-type complex. The figure was produced using MOLSCRIPT (Kraulis, 1991) and rendered with RASTER3D (Merritt and Murphy, 1994).

(B) The binding of NADPH to FabG, FabG[Y151F], and FabG[K155A] as determined by intrinsic NADPH fluorescence as described in Experimental Procedures. The Kd of 3.5 μM for NADPH was calculated from the FabG data.

important since they result in a rearrangement of the active site into a catalytically competent conformation, the removal of potential steric clashes with the cofactor, the formation of a proton relay conduit that is required for the catalytic mechanism, and changes in the quaternary structure of the tetrameric enzyme.

Figure 4 shows the conformational changes that occur in the active site residues Ser138, Tyr151, and Lys155. Upon binding of $NADP^+$, all three residues display significant movements of their α carbon positions and changes in their side chain configurations. The α carbon of Ser138 moves 3.9 Å, and the orientation of the OH group swings around 180° to point up the hydrophobic tunnel that leads to the active site. The space that was previously occupied by Ser138 is now occupied by the OH of Tyr151, whose α carbon moves by a more modest 0.8 Å and whose side chain rotates by 120°. This places the OH oxygen of the Tyr151 side chain in a perfect position to hydrogen bond with the $NADP^+$ via the 2′-hydroxyl on the nicotinamide ribose. The α carbon of Lys155 shifts by 1.1 Å, and the side chain rotates 90° to point toward the active site, allowing the terminal NZ nitrogen to interact directly with the $NADP^+$ by hydrogen bonding with the 2′- and 3′-hydroxyl groups of the nicotinamide ribose.

Residues 87–91 in the β4-α4 loop (labeled "a" in Figure 1B) move to avoid a steric clash with the $NADP^+$ and open up the space for cofactor binding. Specifically, the backbone bond between the C_α and the carbonyl group of Asn86 rotates by 220°, swinging the chain out from the binding cleft and back toward helix α4. In the process, two interactions that stabilize the FabG conforma-

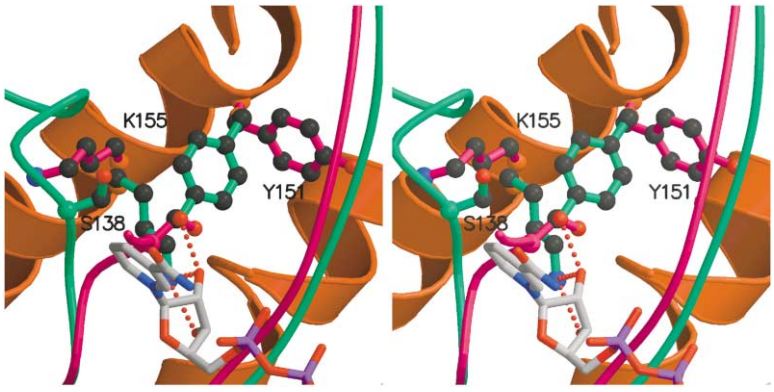

Figure 4. Conformational Changes in the Active Site of FabG upon Binding $NADP^+$

In this stereo view overlay, FabG·$NADP^+$ is shown in green and FabG in magenta. $NADP^+$ is illustrated as a stick figure in its position in the FabG·$NADP^+$ structure, with carbons colored gray, nitrogens blue, oxygens red, and phosphorous purple. Lys155 rotates by 90° to point toward the active site where it hydrogen bonds to the two nicotinamide ribose hydroxyl groups. Ser138 would clash with the incoming cofactor in its apo conformation, and the entire backbone must move away, rotating the side chain in such a way as to point it up toward the incoming substrate. Tyr151 rotates by 90° upon cofactor binding to hydrogen bond with the nicotinamide ribose hydroxyl group on $NADP^+$. This rotation is facilitated by a conformational change in the coil region in front of Tyr151 that moves the main chain toward the α helix in the background. Note that the space occupied by the side chain of Ser138 in FabG becomes occupied by the OH of Tyr151 in the FabG·$NADP^+$ complex. The figure was produced using MOLSCRIPT (Kraulis, 1991) and rendered with RASTER3D (Merritt and Murphy, 1994).

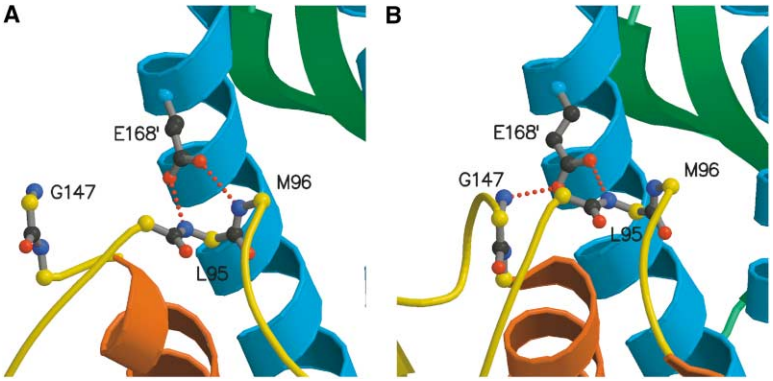

Figure 5. Structural Rearrangements Explain the Allosteric Behavior of FabG

In the two panels, the α helices of monomer A are orange, the β strands and coils of monomer A are yellow, the α helices of monomer B are blue, and the β strands and coils of monomer B are green.

(A) A close up of the FabG intermonomer interface at region "c" as defined in Figure 1B. Glu168′ from one monomer forms hydrogen bonds to the amide nitrogens of Leu95 and Met96 on the adjacent monomer, and residues N-terminal to Gly147 on the β5-α5 loop are disordered.

(B) A close up of the same region in the FabG·NADP$^+$ complex. Note that Glu168′ has shifted its hydrogen bond register to the amide nitrogens of Leu95 and Gly147, and the residues N-terminal to Gly147 on the β5-α5 loop are now ordered. The figure was produced using MOLSCRIPT (Kraulis, 1991) and rendered with RASTER3D (Merritt and Murphy, 1994).

tion of the loop are broken, the hydrophobic packing of Ile89 with Met188 and the hydrogen bond from the backbone amide of Arg91 to the OH group of the active site Tyr151. In FabG, this active site residue is inserted between the β4-α4 loop and the α4 helix, preventing the two secondary structural elements from interacting. When cofactor binds, the side chain of Tyr151 swings 120° out of the way to allow the loop to pack against helix α4 where it forms five new interactions: the hydrophobic packing of Ile89 and Ile106, two hydrogen bonds between the main chain amide nitrogen and carbonyl oxygen of Ile89 and the OD1 and ND2 side chain atoms of Asn110, the hydrophobic packing of Val60 and Ala87, and a salt bridge between Arg91 and Asp105.

Residues 141–146 in the β5-α5 loop (labeled "b" in Figure 1B) are disordered in the FabG structure but form a short helix-turn structure that packs against the antiparallel helices α5 and α5′ (where a prime indicates protein elements from the opposing monomer) at the monomer-monomer interface in the FabG·NADP$^+$ quaternary structure. In the FabG structure, the conformation of the "loose ends" of the disordered segment is secured by a hydrogen bond between the main chain carbonyl oxygen of Val139 and the NE2 nitrogen of Gln148. In the binary complex, this interaction is broken, the two "loose ends" are driven apart, and the disordered loop is pulled in to pack against the surface of the protein. The ends of the newly formed helix-turn structure are secured by two hydrogen bonds between the main chain carbonyl oxygen of Ser138 and the main chain amide nitrogen of Gly141 and between the main chain amide nitrogen of Asn93 and the main chain carbonyl oxygen of Gly147. This newly formed helix-turn region is further stabilized by three new monomer-monomer hydrogen bonding interactions across the dimer interface: the NZ nitrogen of Lys163′ to the main chain carbonyl oxygen of Thr142, the NE nitrogen of Arg167′ to the main chain carbonyl oxygen of Met143, and the OE1 oxygen of Glu168′ to the main chain amide nitrogen of Gly147.

The monomer-monomer interface centered on and mediated by Glu168′ displays a subtle but significant rearrangement upon cofactor binding that is shown in Figure 5 (region "c" in Figure 1B). In this region of the quaternary structure, the β4-α4 loop is secured by interactions with the base of the opposing α5′ that contains the Glu168′ residue. In the FabG structure, the carboxylate group of Glu168′ hydrogen bonds to the backbone amide nitrogens of Leu95 and Met96 (Figure 5A). Upon NADP$^+$ binding, the interactions of Glu168′ shift register, and the carboxylate group of Glu168′ now hydrogen bonds to the backbone amide nitrogens of Leu95 and Gly147 (Figure 5B). This has the effect of pulling the β4-α4 loop "upward" and toward helix α4 (Figure 5B).

Ca^{2+}-FabG Interactions

The FabG·NADP$^+$ complex contains eight Ca^{2+} ions. The presence of the calcium does not alter the structure of the protein in a significant way, because crystals of the same form also grew in a crystallization buffer not containing calcium. These crystals diffracted to lower resolution, but the structure was solved and was identical to the calcium-containing form, except for the absence of electron density in the calcium binding sites. Because the structures were the same, the lower resolution, non-calcium-containing structure is not reported. The locations of these Ca^{2+} ions suggest that they stabilize both the structure itself and the crystal lattice.

Two of the Ca^{2+} ions are involved in very similar crystal contacts and link together the main chain carbonyl oxygens of residues 50 and 53 in the turn between helix α2 and strand β3 with the side chain of Asp194 from a neighboring molecule via a lattice of hydrogen bonded water molecules. Two other Ca^{2+} ions are located in identical environments on the 2-fold symmetry axes of the tetramer that link molecules A and D, and B and C, and each coordinates the OE2 atom of Glu233 and the main chain carbonyl oxygen of Thr234 on strand β7 with their partners on strand β7′. These latter two cations appear to generate minor differences between the FabG·NADP$^+$ and apo FabG structures at the C terminus that is adjacent to this dimer interface. Specifically, the final three residues of the sequence (242–244) are visible in the binary complex but disordered in FabG. They are stabilized by two hydrogen bonds involving the main chain carbonyl oxygen of Val244, one to a water network that is coordinated to the Ca^{2+} ion and a second to the NZ atom of Lys163′ on the opposing monomer.

The final four Ca^{2+} ions are positioned at equivalent locations within the tetramer, directly in the entrances

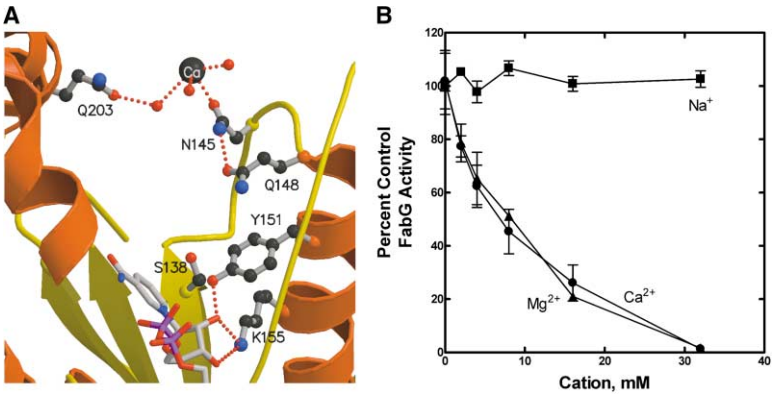

Figure 6. The Divalent Cation Binding Site in FabG·NADP$^+$

(A) A close-up view of the active site of the FabG·NADP$^+$ complex that includes the Ca^{2+} binding site. The Ca^{2+} is coordinated by the OD1 oxygen of Asn145 on one side of the active site entrance and a network of waters stabilized by Gln203 on the opposite side of the entrance. Note the ordered β5-α5 loop between Ser138 and Gln148 that includes Asn145. The figure was produced using MOLSCRIPT (Kraulis, 1991) and rendered with RASTER3D (Merritt and Murphy, 1994).

(B) Divalent cations inhibit FabG activity. The assays were performed using the spectrophotometric assay described in Experimental Procedures.

to the tunnels that lead to the four active sites. This calcium cation binding site is shown in Figure 6A. Each is held in place by coordinate bonds to the OD1 oxygen of Asn145 and a lattice of water molecules. One of these water molecules forms a second hydrogen bond interaction across the active site entrance to the OE1 atom of Gln203 located in the α6/α7 subdomain. These structural data suggested that divalent cations may inhibit FabG activity by obstructing access to the active site. Indeed, divalent cations blocked FabG activity in vitro, whereas increasing the ionic strength in the assay with monovalent ions did not (Figure 6B). This indicates that the structure showing Ca^{2+} blocking the entrance to the active site (Figure 6A) is relevant in solution.

Conformational Changes Create a Proton Circuit

Our FabG·NADP$^+$ structure reveals a linear network of four linked water molecules leading away from the active site that make well defined hydrogen bonded interactions to the protein (Figure 7). The network starts directly at the active site where the first water molecule interacts with the NZ nitrogen of Lys155 and the backbone carbonyl oxygen of Asn110. The second water in the chain is held in place by the main chain carbonyl oxygens of Asn85 and Ala87, and the third water is fixed by the side chain oxygen of Ser113. The fourth and final water associates with the side chain oxygens of Thr11 and Asn85. The water chain is completely contained within the complex, largely buried under the β4-α4 loop and the adenine moiety of the bound cofactor. The conserved Asn110 plays a crucial role in maintaining the integrity of the network by supplying a key carbonyl oxygen, and the residue is rigidly held in place by the two hydrogen bonding interactions between its side chain and the backbone amide nitrogen and carbonyl oxygen of Ile89 that are formed when the β4-α4 loop moves to pack against the α4 helix. It is essential that Asn110 is located at a kink in helix α4 (Figure 1A) because it releases the backbone carbonyl of Asn110 from its normal α-helical hydrogen bonding configuration, allowing it to participate in the formation of the proton wire.

The water network is missing in the structures of apo FabG and FabG[Y151F]·NADP$^+$, with the sole exception being the final water that is present in the FabG[Y151F]·NADP$^+$ complex. The absence of the network in these two structures is not surprising, since its stabilization depends on the conformational changes associated with a correctly bound cofactor. In the FabG[Y151F]·NADP$^+$ complex, the nicotinamide ribose is missing which removes the surrounding 2′ and 3′ hydroxyls and allows access to the exterior. In the FabG structure, the complete absence of cofactor allows solvent access from two directions, and the conformational changes at the active site directly remove some of the key network interactions. Specifically, the rotated Lys155 can no longer initiate the network, the carbonyl oxygen of Ala87 within the shifted β4-α4 loop is no longer available, and the movement of the β4-α4 loop serves to further expose the network to solvent.

Discussion

Mechanism and Function of Cofactor-Induced Conformational Changes

Our structural and biochemical data clearly show that the binding of cofactor to FabG results in a number of conformational changes that activate the enzyme for catalysis. The conformational changes include a complete reorientation of the active site residues from a noncompetent to a competent constellation of catalytic side chains, alterations in the protein backbone to provide the necessary space within the active site for the cofactor to bind by removing steric clashes, and the establishment of a proton wire. A comparison of the FabG structure to the FabG·NADP$^+$ complex reveals that two steric clashes between the cofactor and the FabG would occur if these conformational changes did not take place. The first steric clash is with the N terminus of the β4-α4 loop (region "a" in Figure 1B), and the rotation of the backbone that relieves this clash upon cofactor binding results in both a reorientation of the Tyr151 side chain to point it toward the active site (Figure 4) and an upward motion of the β4-α4 loop (Figure 5). The second steric clash is between the nicotinamide "end" of the cofactor and the N-terminal portion of the β5-α5 loop, directly at the reoriented active site residue Ser138.

Note that the binding of the adenine moiety of NADPH is sufficient to relieve the first clash and cause all of the structural changes. This is clear from a comparison of the FabG·NADP$^+$ structure with the FabG[Y151F]·NADP(H) structure. In the latter complex, the same conformational change has occurred even though the nicotin-

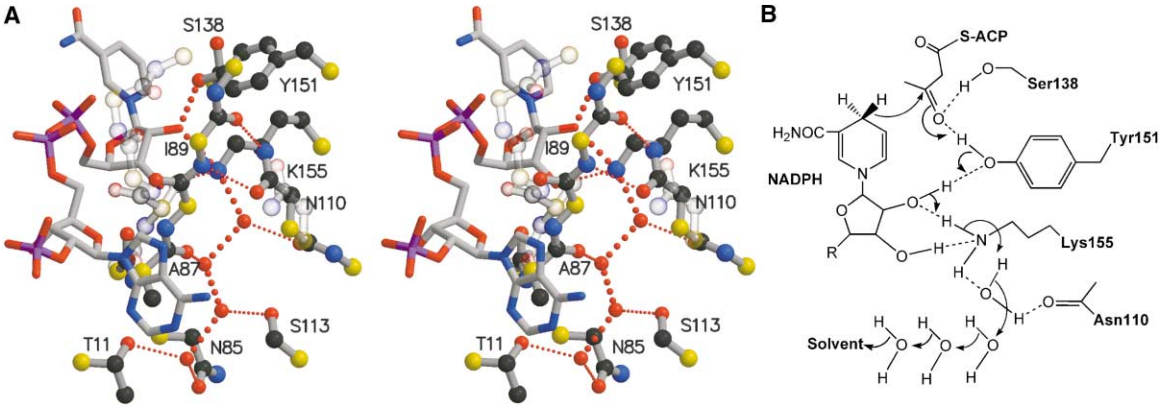

Figure 7. The Proton Relay Water Network and the Catalytic Mechanism of FabG

(A) Stereo view of the active site of the FabG·NADP$^+$ complex showing the active site residues and the water network as ball-and-stick figures, and NADP$^+$ represented as bonds. α-carbons are yellow throughout. The water chain is hydrogen bonded to Lys155 at the top, passes through a number of specific interactions with surrounding residues, and is anchored at the bottom by Thr11 and Asn85 (see text for details). Cofactor binding triggers a large conformational change in the β4-α4 loop, and the locations of residues 87–90 within the loop in the apo FabG structure are shown superimposed as a transparent ball-and-stick representation. The interaction between Asn110 and Ile89, the key to establishing the water network, is broken in the absence of bound cofactor, leading to movement of the β4-α4 loop which dissolves the network. Note also that the adenine moiety of bound NADP$^+$ lies on top of the network to insulate it from solvent. The figure was produced using MOLSCRIPT (Kraulis, 1991) and rendered with RASTER3D (Merritt and Murphy, 1994).

(B) Diagram of the FabG reductase mechanism. Ser138 and Tyr151 form hydrogen bonds to the ketone at the C3 of the substrate. NADPH donates a hydride to the C3 carbon of the substrate, and a proton is transferred to the oxygen from the hydroxyl group of Tyr151. The Tyr151 proton is replenished by a proton relay system through Lys155, the ribose hydroxyls, and a chain of four water molecules that communicate with solvent.

amide end of the cofactor is not bound within the active site (Figure 3) and no steric interference exists between the cofactor and Ser138. The crucial switch that initiates the conformational changes most likely occurs at the N-terminal end of the β4-α4 loop that forms the "back" of the adenine binding pocket (Figure 2). As noted earlier, the backbone of Asn86 rotates by 220° to cause the movement of the β4-α4 loop, and the immediate result is the completion of the adenine pocket (Figure 2), which, presumably, stabilizes its binding.

A comparison of the wild-type and mutant FabG-cofactor structures also demonstrates the importance of Tyr151 in stabilizing the productive binding mode of cofactor, i.e., the conformation that has the nicotinamide moiety in the active site. This structural role for Tyr151 in NADPH binding is reflected by the absence of high-affinity NADPH binding to FabG[Y151F] (Figure 3B). This, in turn, suggests that cofactor binding occurs in two stages. First, the adenine end binds tightly in its pocket, and this is sufficient to cause the conformational changes since they are present in the FabG[Y151F]·NADP(H) structure where only this end is bound. Second, the nicotinamide end is now able to bind at the reorganized active site in which the necessary hydrogen bonding groups, including the OH of Tyr151, are correctly oriented. We propose, therefore, that the conformation of the cofactor in the FabG[Y151F]·NADP(H) complex is mechanistically significant and represents the first stage of cofactor binding.

This two-stage binding mechanism is consistent with the electron density of the cofactor in the FabG·NADP$^+$ complex, in which the adenine end is significantly better defined than the nicotinamide end. The electron density also suggests that the oxidized form of the nicotinamide ring has a lower affinity for the binding pocket than the reduced form. Upon oxidation of NADPH, the nicotinamide ring becomes planar and positively charged, and both transformations may adversely affect the affinity of the cofactor for the enzyme. Since the nicotinamide binding pocket is hydrophobic, we suggest that the acquisition of positive charge is a principal factor. This effect is beneficial to the progression of the catalytic cycle, since oxidized cofactor is more easily expelled from the active site.

Catalysis and the Proton Relay System

The FabG catalytic reduction mechanism requires that a hydride be added to the C3 carbon of the β-ketoacyl-ACP from the nicotinamide ring of NADPH and that a proton be donated to the oxygen on C3 from the OH group of the active site Tyr151. The latter proton needs to be replenished, and in most previous SDR mechanisms, the catalytic lysine is envisioned as protonated and responsible for replenishing the proton lost from Tyr151. However, the large conformational change that occurs upon cofactor binding in FabG buries the Lys155, and in the absence of a suitable counter ion in the structure, it is likely that Lys155 is not charged. We propose that in FabG, the proton is shuttled via a water network that is ideally positioned to serve as a proton wire to the tyrosine via Lys155 and the 2′-hydroxyl on the nicotinamide ribose (Figure 7). Our FabG·NADP$^+$ structure reveals a chain of four hydrogen bonded water molecules linked to the NZ atom of the active site Lys155. This network is characteristic of a proton relay system or "proton wire" that functions to replenish protons used in enzyme catalysis (Meyer, 1992; Pomes and Roux, 2002). A similar proton wire that functions to replenish

the proton extracted from the OH of the active site tyrosine during the catalytic reduction is observed in other SDR enzymes (Filling et al., 2002).

It was recently proposed that the essential and conserved Asn110 is the key to the integrity of the water network and should be regarded as a bone fide active site residue (Oppermann et al., 2003). We prefer to regard the asparagine as an essential structural residue since it does not directly participate in catalysis and it is the backbone carbonyl that participates in the proton wire (Figure 7A). Rather, the kink in helix α4 (Figure 1A) is the essential and conserved structural element since it switches the backbone carbonyl oxygen of Asn110 from hydrogen bonding in the α helix to the water network. In FabG, and some other SDR enzymes, the kink is generated by the side chain OG of a serine residue (Ser113 in FabG) that intercalates into the α-helical hydrogen bonding scheme (Filling et al., 2002; Oppermann et al., 2003). In many other SDR enzymes, the kink results from a glycine at this position which presumably introduces the necessary flexibility into the helix (Filling et al., 2002; Oppermann et al., 2003).

It is clear from our studies that the formation of the proton wire requires a correctly bound cofactor. It is not present in FabG, and only the most distal water from the active site is present in the FabG[Y151F]·$NADP^+$ complex where the nicotinamide half of the cofactor is unbound at the active site. These findings lead to a scenario in which the proton wire is created and dissolved by the conformational changes that accompany the catalytic cycle of cofactor binding and release.

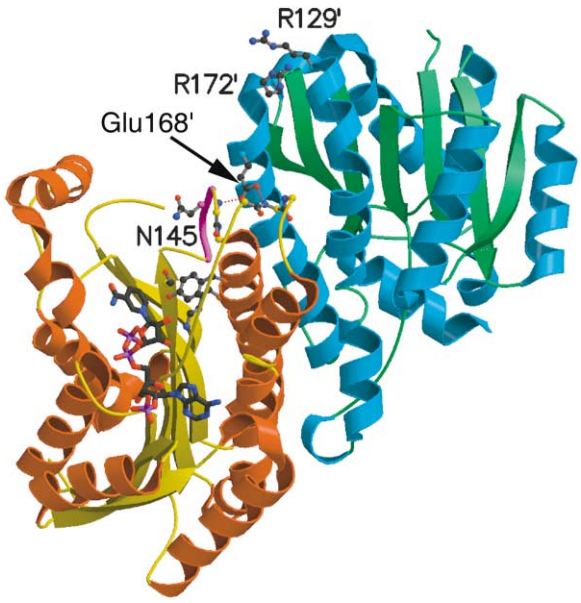

Figure 8. An Overview of the Interacting Monomers in the FabG·$NADP^+$ Complex

Glu168′ and its hydrogen bonding interactions, as depicted in Figure 5B, are shown at the interface. Shown in monomer A are the bound cofactor, the active site residues, the ordered β5-α5 loop (purple), and Asn145, which we propose may interact with the incoming pantetheine moiety of the ACP-bound substrate. Shown in monomer B are Arg129′ and Arg172′, which interact with the incoming ACP (Zhang et al., 2003b). The figure was produced using MOLSCRIPT (Kraulis, 1991) and rendered with RASTER3D (Merritt and Murphy, 1994).

Allosteric Mechanisms in FabG

FabG is an allosteric enzyme whereby the binding of NADPH to one site increases the affinity at that site for the ACP-bound substrate and decreases the affinity for the cofactor at other sites (Price et al., 2001). Structural pathways through which this cooperative transition operates are suggested by our data. Based on computational docking and mutagenesis (Zhang et al., 2001, 2003a), we postulate that an important interaction between ACP and its binding partners involves acidic residues of ACP and conserved arginines on the enzymes of type II fatty acid synthesis. Mutagenesis and NMR spectroscopy demonstrate that Arg129 and Arg172 play a key role in ACP-FabG interactions and are essential to form the docking site for ACP on FabG (Zhang et al., 2003b). Figure 8 shows that the FabG ACP binding site is closest to the active site of an adjacent monomer in the tetramer and that substrate delivery via the pantetheine arm of ACP would take place across the dimer interface. This arrangement is typical for an allosteric enzyme because small movements in the quaternary structure across a monomer-monomer interface can have a large effect at the active site. Using the distance between the α carbons of Arg172′ and Ile136 as a ruler to approximate the distance between the ACP binding site and the base of the active site cleft shows that the former moves toward the latter by ~1.3 Å upon cofactor binding, a small but significant amount. Also shown in Figure 8 is the location of Glu168′, which changes its hydrogen bonding register upon cofactor binding and is located directly between the ACP binding site and the active site on the dimer interface. We suggest that the conformational changes that occur during NADPH binding switch the hydrogen bonding of Glu168 to alter the associated interface as described earlier and facilitate substrate delivery by the adjacently bound ACP.

The data also point to an important role for the ordering of the β5-α5 loop upon cofactor binding in orienting the pantetheine moiety of the incoming acyl-ACP substrate. The β5-α5 loop is positioned directly between the active site and arginines 129′ and 172′ located on the adjacent monomer (Figure 8). Modeling studies of the binding of FabG and ACP (data not shown) suggest that the distal end of the pantetheine must traverse the ordered β5-α5 loop in order to reach the active site and deliver its substrate. The location of the conserved Asn145 in the β5-α5 loop (Figure 8) suggests that it may have a specific role in binding the pantetheine moiety in the ternary complex. This residue is conserved in 14 out of 18 FabG sequences examined, and one of the exceptions is a conservative substitution (glutamine). The other three substitutions are leucines that are only present in *Mycobacterial* enzymes involved in the unique synthesis of very long-chain fatty acids and may have a specialized role in substrate specificity (Cohen-Gonsaud et al., 2002). We have identified similar conserved polar residues (threonines) in the pantetheine binding pocket of the type II β-ketoacyl-ACP synthases (Price et al., 2003). Calcium inhibition of FabG supports a role

for this region in substrate binding, since the Ca^{2+} ion that is bound near the active site in the FabG·$NADP^+$ complex interacts directly with Asn145.

Comparison to Other FabGs

The structure of FabG has also been determined from two other organisms, *Mycobacterium tuberculosis* and *Brassica napus*. These structures support our findings on the *E. coli* enzyme and provide additional insights into the conformational changes that accompany the FabG catalytic mechanism. A comparison of the *E. coli* FabG structure (Price et al., 2001) to ligand-free enzyme from *M. tuberculosis* (mtFabG1) (Cohen-Gonsaud et al., 2002) shows many similarities and few potentially important differences. The active site of mtFabG1 without bound cofactor shows identical conformations in the Ser-Tyr-Lys triad that are not conducive to catalysis. The β5-α5 loop in mtFabG1 is also disordered, but an additional feature is a more disordered β4-α4 loop.

A comparison of the *E. coli* FabG·$NADP^+$ structure to that of the FabG·$NADP^+$ binary complex from *B. napus* (bnFabG) (Fisher et al., 2000) shows that the active site, the β4-α4 loop, and the β5-α5 loop all adopt the same conformation. However, the α6/α7 subdomain is in a relatively open conformation in the *E. coli* structure, while it is in a more closed conformation in the *B. napus* structure. This permits a more extensive protein-cofactor interface at the nicotinamide end in bnFabG·$NADP^+$, which presumably stabilizes the complex relative to the *E. coli* complex. Consistent with this, the electron density for the nicotinamide moiety of the cofactor in our *E. coli* FabG·$NADP^+$ complex is weaker than for the adenine end. The bnFabG·$NADP^+$ complex suggests that a further conformational change occurs upon binding of the second substrate (acyl-ACP) to the *E. coli* protein that involves a closing of the α6/α7 subdomain over the active site pocket. We have noted that the α6/α7 subdomain appears to be the most flexible region of the molecule based on higher overall temperature factors, and the subdomain does show some movement relative to the body of the protein when cofactor binds. This proposal is consistent with the structure of another SDR enzyme, 7α-hydroxysteroid dehydrogenase, in complex with NAD^+ and hydroxysteroid substrate, which shows a closed substrate binding loop in a region homologous to the α6/α7 subdomain (Tanaka et al., 1996).

Summary and Conclusions

Our work defines the conformational changes that directly control the biochemical properties and catalytic mechanism of *E. coli* FabG. FabG has a sequential, ordered kinetic mechanism, with the NADPH cofactor as the leading substrate and $NADP^+$ as the last product to leave (Fawcett et al., 2000; Price et al., 2001). Cofactor binding to FabG is a two-step process that results in major conformational changes that are important for the correct ordered progression of the catalytic mechanism. The adenine and its associated ribose are the first elements to bind some distance from the active site. This initial event leads to a reorganization of the active site, the ordering of main chain elements close to the active site, and changes at the dimer interface. The nicotinamide end of the cofactor then binds to the correctly configured active site and completes the creation of a proton wire, which represents the final crucial element of the active site. The movement of the interface and the ordering of the β5-α5 loop allow the acyl-ACP substrate access to the active site, and data from the *B. napus* binary complex suggest that the α6/α7 subdomain rotates to enclose the active site as the final step in the formation of the ternary complex. The closing of the α6/α7 subdomain would create a well-defined entrance tunnel to the active site, and analogous tunnels in other FAS II enzymes appear to play an important role in binding the pantetheine moiety of the acyl-ACP substrate (Davies et al., 2000; Price et al., 2003; Qiu et al., 2001). The negative allostery presumably drives this sequence into reverse when cofactor binds at another site in the tetramer. The reverse sequence would result in the $NADP^+$ leaving the active site last, as observed.

The conformational changes upon cofactor binding that we have described appear to be unique to the FabG members of the extended SDR family. Equivalent changes are not observed in the structures of 3α-hydroxysteroid dehydrogenase (Grimm et al., 2000), GDP-mannose 4,6-dehydratase (Somoza et al., 2000), and 17β-hydroxysteroid dehydrogenase (Ghosh et al., 1995). One possible reason is related to the unique protein substrate (acyl-ACP) with which FabG interacts. When acyl-ACP is bound to FabG, with the pantetheine arm inserted into the active site tunnel, a mechanism to ensure that NADPH is already present at the base of the tunnel would be advantageous. Also, a negative allostery mechanism to disrupt this large substrate complex after catalysis has taken place would appear to be warranted. Both are accommodated by the conformational changes that we describe.

Experimental Procedures

Materials and Standard Methods

Cofactors (NADPH and $NADP^+$) were purchased from Sigma-Aldrich. FabG mutants were prepared by overlapping polymerase chain reaction using the *fabG* expression plasmid as template. FabG [Y151F] was constructed using the 5′-CAGGCCAACTTCGCTGCGG CGAAAGC plus 5′-CGCCGCAGCGAAGTTGGCCTGACCGC primer pair, and FabG[K155A] was generated using the 5′-GCGGCGGCAG CGGGCTTGATCG plus 5′-CAAGCCCGCTGCCGCCGCAGCGTA-GTTG primer pair. The mutated codons are underlined. The DNA sequences were verified by the St. Jude Molecular Resource Center, and the proteins were expressed and purified using the 6× His tag system described previously (Price et al., 2001). NADPH binding assay was the same as described previously (Price et al., 2001) and utilized the increase in intrinsic NADPH fluorescence to signal binding. FabG assays using the β-hydroxybutyryl-CoA substrate analogs were as described previously (Zhang et al., 2003b).

Crystallization

Pure aliquots of both FabG and FabG[Y151F] were dialyzed against a buffer of 20 mM Tris-HCl (pH 7.6), 50 mM NaCl, 1 mM DTT, and 1 mM EDTA and then concentrated to 5 mg/ml. $NADP^+$ (NADPH) was added directly to aliquots of FabG or FabG[Y151F] and gently agitated overnight. The ratio of cofactor molecules to protein monomers was 10:1. Crystals of both complexes were grown using the hanging drop method. The FabG·$NADP^+$ complex used a well solution of 20% PEG-1000, 0.2 M calcium acetate, and 0.1 M Tris-HCl (pH 9.0), and crystals grew to 0.3 mm in 1–2 weeks. The FabG[Y151F]·NADP(H) cocrystals grew in a crystallization buffer of 32.5% PEG-

3350 and 0.1 M CHES (pH 9.5) and grew to 0.2 mm in less than 1 week.

Data Collection and Processing

The crystals were mounted on standard nylon loops, passed through a cryoprotectant of 50% paratone-N, 50% mineral oil, and frozen in the cold nitrogen vapor stream of a cryostat. All data were collected at 100 K using a Nonius FR591 X-ray generator. Data for the FabG·$NADP^+$ cocrystals were measured with a DIP 2030H detector system and integrated using the HKL software package (Otwinowski and Minor, 1997). The integrated data for the wild-type crystal were merged and scaled using SCALEPACK (Otwinowski and Minor, 1997), and the crystals were determined to be in space group $P2_1$. Data for the FabG[Y151F]·NADP(H) cocrystals were measured with a Bruker-Nonius CCD, integrated with SAINT (Bruker AXS), and merged and scaled using PROSCALE (Bruker AXS). The mutant crystals were determined to belong to space group $C222_1$. Statistics for data collection and processing for both crystals are listed in Table 1.

Structure Determination of FabG·$NADP^+$

The structure was solved using the molecular replacement method. The program AMoRe (Navaza, 1994) was used to place a tetramer search model in the asymmetric unit. The search model used was the FabG tetramer structure, which lacks cofactor (Price et al., 2001). Regions of the protein sequence that were predicted to undergo conformational change in the FabG[$NADP^+$] structure compared to the FabG structure (Price et al., 2001) were deleted from the search model in order to reduce bias. All refinements and map calculations were performed with the program CNS v 1.1 (Brünger et al., 1998). Throughout the refinement, $3F_o$-$2F_c$, $2F_o$-F_c, and F_o-F_c maps were examined. Initial maps were calculated after rigid body refinement of the molecular replacement solution. Four cycles of manual rebuilding followed by simulated annealing refinement and map calculation were necessary to build the entire sequence. $NADP^+$ molecules were added to the structure when the electron density corresponding to the cofactor was clearly visible. Waters were added using CNS and were visually inspected for electron density and for H bonding geometry. Incorrectly assigned waters were rejected, and some additional waters were added by hand. Eight strong electron density peaks were initially interpreted as Ca^{2+} ions based on the presence of 0.2 M calcium acetate in the crystallization buffer, and the assignment was subsequently supported by their behavior during refinement and the lack of residual electron density for these peaks in the final maps. The final statistics of the model are compiled in Table 2.

Structure Determination of FabG[Y151F]·NADP(H)

The FabG[Y151F]·NADP(H) structure was solved exactly as described for the FabG·$NADP^+$ cocrystals, except that the FabG dimer (with cofactor removed) from the FabG·$NADP^+$ cocrystal structure was used as the search model. Initial maps calculated after rigid body refinement showed good electron density for almost the entire protein and clear negative density (in the F_o-F_c map) at the hydroxyl oxygen of Tyr151 in both monomers in the asymmetric unit. Two cycles of manual rebuilding followed by simulated annealing refinement and map calculation were needed to refine the structure. When density for cofactor was visible, partial NADPH molecules (lacking nicotinamide and nicotinamide ribose) were built into the structure. The complete cofactor was never visible. Waters were added and inspected as for the FabG structure. The final statistics of the FabG and FabG[Y151F]·NADP(H) models are shown in Table 2.

Acknowledgments

This work was supported by National Institutes of Health grant GM 34496, Cancer Center (CORE) support grant CA 21765, and the American Lebanese Syrian Associated Charities. We thank Matt Frank and Daren Hemingway for their expert assistance and the St. Jude Protein Production Facility for preparation of FabG and preliminary crystallization trials.

Received: October 8, 2003
Revised: November 11, 2003
Accepted: November 14, 2003
Published: March 9, 2004

References

Alberts, A.W., Majerus, P.W., Talamo, B., and Vagelos, P.R. (1964). Acyl carrier protein II. Intermediary reactions of fatty acid synthesis. Biochemistry *3*, 1563–1571.

Brünger, A.T., Adams, P.D., Clore, G.M., DeLano, W.L., Gros, P., Grosse-Kunstleve, R.W., Jiang, J.S., Kuszewski, J., Nilges, M., Pannu, N.S., et al. (1998). Crystallography & NMR system: a new software suite for macromolecular structure determination. Acta Crystallogr. D Biol. Crystallogr. *54*, 905–921.

Campbell, J.W., and Cronan, J.E., Jr. (2001). Bacterial fatty acid biosynthesis: targets for antibacterial drug discovery. Annu. Rev. Microbiol. *55*, 305–332.

Cohen-Gonsaud, M., Ducasse, S., Hoh, F., Zerbib, D., Labesse, G., and Quemard, A. (2002). Crystal structure of MabA from *Mycobacterium tuberculosis*, a reductase involved in long-chain fatty acid biosynthesis. J. Mol. Biol. *320*, 249–261.

Cronan, J.E., Jr., and Rock, C.O. (1996). Biosynthesis of membrane lipids In *Escherichia coli* and *Salmonella typhimurium*: Cellular and Molecular Biology, J.L. Ingraham and F.C. Neidhardt, eds. (Washington, D.C: American Society for Microbiology), pp. 612–636. .

Davies, C., Heath, R.J., White, S.W., and Rock, C.O. (2000). The 1.8 Å cystal structure and active site architecture of β-ketoacyl-[acyl carrier protein] synthase III (FabH) from *Escherichia coli.* Structure *8*, 185–195.

Fawcett, T., Copse, C.L., Simon, J.W., and Slabas, A.R. (2000). Kinetic mechanism of NADH-enoyl-ACP reductase from *Brassica napus.* FEBS Lett. *484*, 65–68.

Filling, C., Berndt, K.D., Benach, J., Knapp, S., Prozorovski, T., Nordling, E., Ladenstein, R., Jörnvall, H., and Oppermann, U. (2002). Critical residues for structure and catalysis in short-chain dehydrogenases/reductases. J. Biol. Chem. *277*, 25677–25684.

Fisher, M., Kroon, J.T., Martindale, W., Stuitje, A.R., Slabas, A.R., and Rafferty, J.B. (2000). The X-ray structure of *Brassica napus* β-ketoacyl carrier protein reductase and its implications for substrate binding and catalysis. Structure *8*, 339–347.

Ghosh, D., Pletnev, V.Z., Zhu, D.W., Wawrzak, Z., Duax, W.L., Pangborn, W., Labrie, F., and Lin, S.X. (1995). Structure of human estrogenic 17β-hydroxysteroid dehydrogenase at 2.20 Å resolution. Structure *3*, 503–513.

Grimm, C., Maser, E., Mobus, E., Klebe, G., Reuter, K., and Ficner, R. (2000). The crystal structure of 3α-hydroxysteroid dehydrogenase/carbonyl reductase from *Comamonas testosteroni* shows a novel oligomerization pattern within the short chain dehydrogenase/reductase family. J. Biol. Chem. *275*, 41333–41339.

Heath, R.J., White, S.W., and Rock, C.O. (2001). Lipid biosynthesis as a target for antibacterial agents. Prog. Lipid Res. *40*, 467–497.

Jackowski, S., and Rock, C.O. (2002). Forty years of fatty acid biosynthesis. Biochem. Biophys. Res. Commun. *292*, 1155–1166.

Jörnvall, H., Persson, B., Krook, M., Atrian, S., Gonzalez-Duarte, R., Jeffery, J., and Ghosh, D. (1995). Short-chain dehydrogenases/reductases (SDR). Biochemistry *34*, 6003–6013.

Kraulis, P.J. (1991). MOLSCRIPT: a program to produce both detailed and schematic plots of protein structures. J. Appl. Crystallogr. *24*, 946–950.

Laskowski, R.A., McArthur, M.W., Moss, D.S., and Thornton, J.M. (1993). PROCHECK: a program to check the quality of protein structures. J. Appl. Crystallogr. *26*, 282–291.

Merritt, E.A., and Murphy, M.E.P. (1994). Raster3D version 2.0. A program for photorealistic molecular graphics. Acta Crystallogr. *D50*, 869–873.

Meyer, E. (1992). Internal water molecules and H-bonding in biological macromolecules: a review of structural features with functional implications. Protein Sci. *1*, 1543–1562.

Navaza, J. (1994). AMoRe—an automated package for molecular replacement. Acta Crystallogr. *A50*, 869–873.

Oppermann, U., Filling, C., Hult, M., Shafqat, N., Wu, X., Lindh, M., Shafqat, J., Nordling, E., Kallberg, Y., Persson, B., et al. (2003). Short-chain dehydrogenases/reductases (SDR): the 2002 update. Chem. Biol. Interact. *143–144*, 247–253.

Otwinowski, Z., and Minor, W. (1997). Processing of X-ray diffraction data collected in oscillation mode. Methods Enzymol. *276*, 307–326.

Pomes, R., and Roux, B. (2002). Molecular mechanism of H^+ conduction in the single-file water chain of the gramicidin channel. Biophys. J. *82*, 2304–2316.

Price, A.C., Zhang, Y.-M., Rock, C.O., and White, S.W. (2001). The structure of β-ketoacyl-[acyl carrier protein] reductase from *Escherichia coli*: negative cooperativity and its structural basis. Biochemistry *40*, 12772–12781.

Price, A.C., Rock, C.O., and White, S.W. (2003). The 1.3 Å resolution crystal structure of β-ketoacyl-acyl carrier protein synthase II from *Streptococcus pneumoniae.* J. Bacteriol. *185*, 4136–4143.

Qiu, X., Janson, C.A., Smith, W.W., Head, M., Lonsdale, J., and Konstantinidis, A.K. (2001). Refined structures of β-ketoacyl-acyl carrier protein synthase III. J. Mol. Biol. *307*, 341–356.

Sheldon, P.S., Kekwick, R.G., Smith, C.G., Sidebottom, C., and Slabas, A.R. (1992). 3-Oxoacyl-[ACP] reductase from oilseed rape (*Brassica napus*). Biochim. Biophys. Acta *1120*, 151–159.

Smith, S., Witkowski, A., and Joshi, A.K. (2003). Structural and functional organization of the animal fatty acid synthase. Prog. Lipid Res. *42*, 289–317.

Somoza, J.R., Menon, S., Schmidt, H., Joseph-McCarthy, D., Dessen, A., Stahl, M.L., Somers, W.S., and Sullivan, F.X. (2000). Structural and kinetic analysis of *Escherichia coli* GDP-mannose 4,6 dehydratase provides insights into the enzyme's catalytic mechanism and regulation by GDP-fucose. Structure *8*, 123–135.

Tanabe, T., Tanaka, N., Uchikawa, K., Kabashima, T., Ito, K., Nonaka, T., Mitsui, Y., Tsuru, M., and Yoshimoto, T. (1998). Roles of the Ser146, Tyr159, and Lys163 residues in the catalytic action of 7α-hydroxysteroid dehydrogenase from *Escherichia coli.* J. Biochem. (Tokyo) *124*, 634–641.

Tanaka, N., Nonaka, T., Tanabe, T., Yoshimoto, T., Tsuru, D., and Mitsui, Y. (1996). Crystal structures of the binary and ternary complexes of 7α-hydroxysteroid dehydrogenase from *Escherichia coli.* Biochemistry *35*, 7715–7730.

Toomey, R.E., and Wakil, S.J. (1966). Studies on the mechanism of fatty acid synthesis. XV. Preparation and general properties of β-ketoacyl acyl carrier protein reductase from *Escherichia coli.* Biochim. Biophys. Acta *116*, 189–197.

Zhang, Y., and Cronan, J.E., Jr. (1998). Transcriptional analysis of essential genes of the *Escherichia coli* fatty acid biosynthesis gene cluster by functional replacement with the analogous *Salmonella typhimurium* gene cluster. J. Bacteriol. *180*, 3295–3303.

Zhang, Y.-M., Rao, M.S., Heath, R.J., Price, A.C., Olson, A.J., Rock, C.O., and White, S.W. (2001). Identification and analysis of the acyl carrier protein (ACP) docking site on β-ketoacyl-ACP synthase III. J. Biol. Chem. *276*, 8231–8238.

Zhang, Y.-M., Marrakchi, H., White, S.W., and Rock, C.O. (2003a). The application of computational methods to explore the diversity and structure of bacterial fatty acid synthase. J. Lipid Res. *44*, 1–10.

Zhang, Y.-M., Wu, B., Zheng, J., and Rock, C.O. (2003b). Key residues responsible for acyl carrier protein (ACP) and β-ketoacyl carrier protein reductase (FabG) interaction. J. Biol. Chem., in press.

Accession Numbers

Atomic coordinates have been deposited in the Protein Data Bank under ID codes 1Q7B for the FabG·$NADP^+$ complex and 1Q7C for the FabG[Y151F]·$NADP^+$ complex.